JACS
JOURNAL OF THE AMERICAN CHEMICAL SOCIETY

Subscriber access provided by UNIV OF YORK

Article

Vapochromism and Its Structural Basis in a Luminescent Pt(II) Terpyridine–Nicotinamide Complex

Thaddeus J. Wadas, Quan-Ming Wang, Yong-joo Kim, Christine Flaschenreim, Thomas N. Blanton, and Richard Eisenberg

J. Am. Chem. Soc., **2004**, 126 (51), 16841-16849• DOI: 10.1021/ja047955s • Publication Date (Web): 03 December 2004

Downloaded from http://pubs.acs.org on April 5, 2009

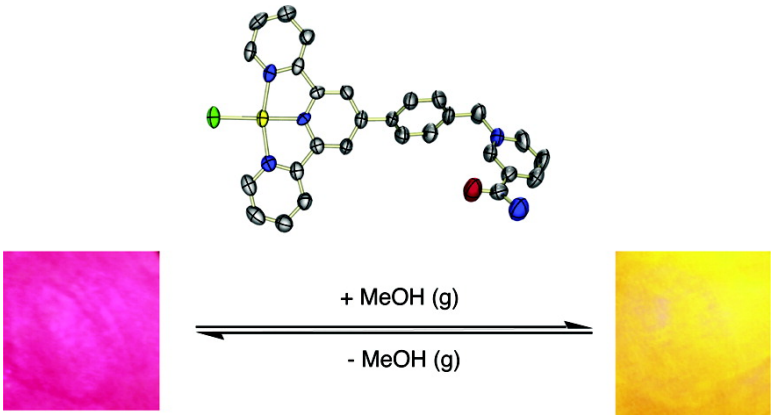

More About This Article

Additional resources and features associated with this article are available within the HTML version:

- Supporting Information
- Links to the 23 articles that cite this article, as of the time of this article download
- Access to high resolution figures
- Links to articles and content related to this article
- Copyright permission to reproduce figures and/or text from this article

View the Full Text HTML

ACS Publications
High quality. High impact.

Journal of the American Chemical Society is published by the American Chemical Society. 1155 Sixteenth Street N.W., Washington, DC 20036

J|A|C|S
ARTICLES
Published on Web 12/03/2004

Vapochromism and Its Structural Basis in a Luminescent Pt(II) Terpyridine−Nicotinamide Complex

Thaddeus J. Wadas, Quan-Ming Wang, Yong-joo Kim, Christine Flaschenreim, Thomas N. Blanton,† and Richard Eisenberg*

Contribution from the Department of Chemistry, University of Rochester, Rochester, New York 14627

Received April 8, 2004; E-mail: eisenberg@chem.rochester.edu

Abstract: A novel Pt(II) terpyridine complex that has a nicotinamide moiety linked to the terpyridyl ligand has been synthesized in good yield and studied structurally and spectroscopically. The complex, [Pt(Nttpy)Cl]$(PF_6)_2$ where Nttpy = 4′-(*p*-nicotinamide-*N*-methylphenyl)-2,2′:6′,2″-terpyridine, is observed to be brightly luminescent in the solid state at room temperature and at 77 K. The complex exhibits reversible vapochromic behavior and crystallographic change in the presence of several volatile organic solvents. Upon exposure to methanol vapors, the complex changes color from red to orange, and a shift to higher energy is observed in the emission maximum with an increase in excited-state lifetime and emission intensity. The crystal and molecular structures of the orange and red forms, determined by single-crystal X-ray diffraction on the *same* single crystal, were found to be equivalent in the molecular sense and only modestly different in terms of packing. In both forms, the cationic Pt(II) complexes possess distorted square planar geometries. Analysis of the orange form's crystal packing reveals the presence of solvent molecules in lattice voids, Pt···Pt separations averaging 3.75 Å and a zigzag arrangement between nearest neighbor Pt atoms, whereas the red form is devoid of solvent within the crystal lattice and contains complexes stacked with a nearly linear arrangement of Pt(II) ions having an average distance of 3.33 Å. On the basis of the crystallographic data, it is evident that sorption of methanol vapor induces a change in intermolecular contacts and Pt···Pt interactions in going from red to orange. Disruption of the d^8-d^8 metallophilic interactions consequently alters the emitting state from ^{3}[(d)$\sigma^*-\pi^*$(terpyridine)] that is formally a metal−metal-to-ligand charge transfer (MMLCT) state in the red form to one in which the HOMO corresponds to a more localized Pt(d) orbital in the red form (^{3}MLCT).

Introduction

Interest in sensor development has grown over the past decade because of the need to develop sensitive systems which detect chemical and biological analytes. Well-defined systems have been reported that specifically detect the presence of cations, anions, transition metal ions, and volatile organic molecules or that measure fluctuations in pH or concentrations of O_2 and CO_2.[1−9] Chemo-sensors of this type generally contain a receptor for binding the species of interest which is covalently attached to a reporting center capable of signaling a positive interaction. For luminescence based sensors, transition metal chromophores such as $Ru(bpy)_3^{2+}$ and tricarbonyl Re(I) polypyridine complexes have most commonly been used as the signaling center in a supramolecular sensor assembly because of their well documented photophysical properties.[9]

More recently, other metal complexes based on Pt(II) have shown promise in sensor development.[10−21] Mann and coworkers have investigated the solid-state structure of a series of square planar Pt(II) complexes that revealed short metal−

† Analytical Technology Division, Eastman Kodak Company, Rochester, New York 14650.

(1) Robertson, A.; Shinkai, S. *Coord. Chem. Rev.* **2000**, *205*, 157−199.
(2) Beer, P. D.; Cadman, J. *Coord. Chem. Rev.* **2000**, *205*, 131−155.
(3) Demas, J. N.; DeGraff, B. A. *Coord. Chem. Rev.* **2001**, *211*, 317−351.
(4) Sun, S.-S.; Lees, A. J. *Coord. Chem. Rev.* **2002**, *230*, 171−192.
(5) Fabbrizzi, L.; Licchelli, M.; Rabaioli, G.; Taglietti, A. *Coord. Chem. Rev.* **2000**, *205*, 85−108.
(6) Parker, D. *Coord. Chem. Rev.* **2000**, *205*, 109−130.
(7) Prodi, L.; Bolletta, F.; Montalti, M.; Zaccheroni, N. *Coord. Chem. Rev.* **2000**, *205*, 59−83.
(8) de Silva, A. P.; Fox, D. B.; Huxley, A. J. M.; Moody, T. S. *Coord. Chem. Rev.* **2000**, *205*, 41−57.
(9) Keefe, M. H.; Benkstein, K. D.; Hupp, J. T. *Coord. Chem. Rev.* **2000**, *205*, 201−228.
(10) Exstrom, C. L.; Sowa, J. R., Jr.; Daws, C. A.; Janzen, D.; Mann, K. R.; Moore, G. A.; Stewart, F. F. *Chem. Mater.* **1995**, *7*, 15−17.
(11) Daws, C. A.; Exstrom, C. L.; Sowa, J. R., Jr.; Mann, K. R. *Chem. Mater.* **1997**, *9*, 363−368.
(12) Kunugi, Y.; Mann, K. R.; Miller, L. L.; Exstrom, C. L. *J. Am. Chem. Soc.* **1998**, *120*, 589−590.
(13) Exstrom, C. L.; Pomije, M. K.; Mann, K. R. *Chem. Mater.* **1998**, *10*, 942−945.
(14) Kunugi, Y.; Miller, L. L.; Mann, K. R.; Pomije, M. K. *Chem. Mater.* **1998**, *10*, 1487−1489.
(15) Buss, C. E.; Anderson, C. E.; Pomije, M. K.; Lutz, C. M.; Britton, D.; Mann, K. R. *J. Am. Chem. Soc.* **1998**, *120*, 7783−7790.
(16) Drew, S. M.; Janzen, D. E.; Buss, C. E.; MacEwan, D. I.; Dublin, K. M.; Mann, K. R. *J. Am. Chem. Soc.* **2001**, *123*, 8414−8415.
(17) Buss, C. E.; Mann, K. R. *J. Am. Chem. Soc.* **2002**, *124*, 1031−1039.
(18) Grate, J. W.; Moore, L. K.; Janzen, D. E.; Veltkamp, D. J.; Kaganove, S.; Drew, S. M.; Mann, K. R. *Chem. Mater.* **2002**, *14*, 1058−1066.
(19) Drew, S. M.; Janzen, D. E.; Mann, K. R. *Anal. Chem.* **2002**, *74*, 2547−2555.
(20) Mann, K. R.; Lewis, N. S.; Miskowski, V. M.; Erwin, D. K.; Hammond, G. S.; Gray, H. B. *J. Am. Chem. Soc.* **1977**, *99*, 5525−5526.
(21) Lu, W.; Chan, M. C. W.; Zhu, N. Y.; Che, C. M.; He, Z.; Wong, K. Y. *Chem: A Euro. J.* **2003**, *9*, 6155−6166.

metal distances resulting from notable Pt···Pt interactions.[15] Significant shifts in the solid-state emission maxima of these complexes were reported in the presence of organic solvent vapors, and these vapochromic shifts were thought to occur through noncovalent interactions including hydrogen bonding and lipophilic interactions that affected the Pt···Pt distances through lattice expansion and contraction. Several neutral complexes of the formula $[Pt(CN\text{-}p\text{-}(C_2H_5)C_6H_4)_2(CN)_2]$ were also found to display vapochromic behavior, and structural analyses of these complexes revealed short Pt···Pt distances and large channels in the solid-state capable of accommodating solvent molecules.[17] Powder diffraction studies demonstrated that upon exposure to solvent vapors, considerable expansion of the crystal lattice occurred while a blue-shift was seen in the emission spectra. For both sets of complexes, the vapochromic behavior was reproducible and reversible. Recently, vapochromism has been reported for a thallium−gold(I) system as well.[22]

Although Pt double salts have shown promise in the development of sensor based technologies, several disadvantages do exist. They often crystallize as pseudo-polymorphs in the form of different solid-state hydrates that can make purification difficult. Additionally, these polymorphic forms may not have the desired vapochromic properties. Finally, complexes that are water soluble are difficult to cast in thin films while those that are soluble in organic solvents lack the desired sensitivity needed in sensor based applications.

Platinum polypyridine complexes have the potential to be more useful in the development of sensor technology since they display interesting solution and solid-state photoluminescence properties which are derived from ^{3}IL, ^{3}MLCT, and ^{3}MMLCT excited states.[23−31] Unlike the first two, a ^{3}MMLCT (metal−metal-to-ligand charge transfer) excited-state arises when two Pt(II) polypyridine complexes are in close proximity to allow for metallophilic interaction between d_{z^2} and p_z orbitals of neighboring Pt centers.[32−34] These interactions often generate photoluminescence that is lower in energy than a ^{3}MLCT emission and can be eliminated by removal of the weak Pt···Pt interactions.[35−37] In this context, Pt terpyridine complexes appear especially appealing because the ligands are easily derivatized and they show interesting and varied photophysical properties in the solid state and in solution.[32,38−57] On the basis of published reports, it was thought that $Pt(trpy)Cl^+$ systems would be interesting to examine regarding sensing applications if the emission properties arising from ^{3}MLCT and ^{3}MMLCT excited states could be influenced by external molecular species and analytes.

The present paper reports the synthesis, structural characterization, and solid-state photophysical properties of a novel Pt terpyridine complex that displays a selective and reversible vapochromic response toward a limited number of organic solvents. A distinction from prior studies on vapochromic behavior is that the present investigation includes the X-ray structural characterization of both red and orange forms of the complex determined on the *same* single crystal and thus provides interesting detail on the basis of the vapochromic effect in the title compound. The results clearly show that the crystalline state possesses significant enough flexibility to allow expansion and contraction of the lattice with resultant slippage in stacking of planar complexes to affect the metallophilic interactions and consequent emission behavior.

Experimental Section

Materials. The compounds 4′-*p*-tolyl-2,2′:6′,2″-terpyridine (ttpy), nicotinamide, anhydrous methanol, ethanol, biotech grade *N*,*N*′-dimethylformamide, potassium bromide (all from Aldrich), potassium tetrachloroplatinate (Strem Chemical), poly-methyl methacrylate (average MW = 33 000) (PMMA) (Scientific Polymer Products, Inc.) and indium tin oxide (ITO) coated glass (Aldrich) were used without further purification. 4′-(*p*-bromomethylphenyl)-2,2′:6′2″-terpyridine (Br-ttpy) and $Pt(DMSO)_2Cl_2$ were prepared according to literature procedures.[58−60] Syntheses were performed under Ar with degassed solvents purified

(22) Fernandez, E. J.; Lopez-de-Luzuriaga, J. M.; Monge, M.; Montiel, M.; Olmos, M. E.; Perez, J.; Laguna, A.; Mendizabal, F.; Mohamed, A. A.; Fackler, J. P., Jr. *Inorg. Chem.* **2004**, *43*, 3573−3581.
(23) Connick, W. B.; Marsh, R. E.; Schaefer, W. P.; Gray, H. B. *Inorg. Chem.* **1997**, *36*, 913−922.
(24) Connick, W. B.; Henling, L. M.; Marsh, R. E.; Gray, H. B. *Inorg. Chem.* **1996**, *35*, 6261−6265.
(25) Houlding, V. H.; Miskowski, V. M. *Coord. Chem. Rev.* **1991**, *111*, 145−152.
(26) Miskowski, V. M.; Houlding, V. H.; Che, C.-M.; Wang, Y. *Inorg. Chem.* **1993**, *32*, 2518−2524.
(27) Miskowski, V. M.; Houlding, V. H. *Inorg. Chem.* **1989**, *28*, 1529−1533.
(28) Hissler, M.; Connick, W. B.; Geiger, D. K.; McGarrah, J. E.; Lipa, D.; Lachicotte, R. J.; Eisenberg, R. *Inorg. Chem.* **2000**, *39*, 447−457.
(29) Wadas, T. J.; Lachicotte, R. J.; Eisenberg, R. *Inorg. Chem.* **2003**, *42*, 3772−3778.
(30) Whittle, C. E.; Weinstein, J. A.; Geore, M. W.; Schanze, K. S. *Inorg. Chem.* **2001**, *40*, 4053−4062.
(31) Grove, L. J.; Rennekamp, J. M.; Jude, H.; Connick, W. B. *J. Am. Chem. Soc.* **2004**, *126*, 1594−1595.
(32) Tzeng, B.-C.; Fu, W.-F.; Che, C.-M.; Chao, H.-Y.; Cheung, K.-K.; Peng, S.-M. *J. Chem. Soc., Dalton Trans.: Inorg. Chem.* **1999**, 1017−1024.
(33) Roundhill, D. M.; Gray, H. B.; Che, C. M. *Acc. Chem. Res.* **1989**, *22*, 55−61.
(34) Lai, S.-W.; Lam, H.-W.; Lu, W.; Cheung, K.-K.; Che, C. M. *Organometallics* **2002**, *21*, 226−234.
(35) Kishi, S.; Kato, M. *Mol. Cryst. Liq. Cryst. Sci. Technol., Sect. A.* **2002**, *379*, 303−308.
(36) Kato, M.; Omura, A.; Toshikawa, A.; Kishi, S.; Sugimoto, Y. *Angew. Chem., Int. Ed.* **2002**, *41*, 3183−3185.
(37) Che, C.-M.; Fu, W.-F.; Lai, S.-W.; Hou, Y.-J.; Liu, Y.-L. *J. Chem. Soc.: Chem. Commu.* **2003**, 118−119.
(38) Bailey, J. A.; Hill, M. G.; Marsh, R. E.; Miskowski, V. M.; Schaefer, W. P.; Gray, H. B. *Inorg. Chem.* **1995**, *34*, 4591−4599.
(39) Bailey, J. A.; Miskowski, V. M.; Gray, H. B. *Inorg. Chem.* **1993**, *32*, 369−370.
(40) Arena, G.; Calogero, G.; Campagna, S.; Scolaro, L. M.; Ricevuto, V.; Romeo, R. *Inorg. Chem.* **1998**, *37*, 2763−2769.
(41) Buchner, R.; Cunningham, C. T.; Field, J. S.; Haines, R. J.; McMillin, D. R.; Summerton, G. C. *J. Chem. Soc., Dalton Trans.: Inorg. Chem.* **1999**, 711−718.
(42) Buchner, R.; Field, J. S.; Haines, R. J.; Cunningham, C. T.; McMillin, D. R. *Inorg. Chem.* **1997**, *36*, 3952−3956.
(43) Field, J. S.; Haines, R. J.; McMillin, D. R.; Summerton, G. C. *J. Chem. Soc., Dalton Trans.* **2002**, 1369−1376.
(44) Cortes, M.; Carney, J. T.; Oppenheimer, J. D.; Downey, K. E.; Cummings, S. D. *Inorg. Chim. Acta* **2002**, *333*, 148−151.
(45) Field, J. S.; Gertenbach, J.-A.; Haines, R. J.; Ledwaba, L. P.; Mashapa, N. T.; McMillin, D. R.; Munro, O. Q.; Summerton, G. C. *Dalton Trans.* **2003**, 1176−1180.
(46) Lai, S.-W.; Chan, M. C. W.; Cheung, K.-K.; Che, C.-M. *Inorg. Chem.* **1999**, *38*, 4262−4267.
(47) Hui, C.-K.; Chu, B. W.-K.; Zhu, N.; Yam, V. W.-W. *Inorg. Chem.* **2002**, *41*, 6178−6180.
(48) Michalec, J. F.; Bejune, S. A.; McMillin, D. R. *Inorg. Chem.* **2000**, *39*, 2708−2709.
(49) McMillin, D. R.; Moore, J. J. *Coord. Chem. Rev.* **2002**, *229*, 113−121.
(50) Yam, V. W.-W.; Tang, R. P.-L.; Wong, K. M.-C.; Ko, C.-C.; Cheung, K.-K. *Inorg. Chem.* **2001**, *40*, 571−574.
(51) Yam, V. W.-W.; Wong, K. M.-C.; Zhu, N. *Angew. Chem., Int. Ed.* **2003**, *42*, 1400−1403.
(52) Yip, H. K.; Cheng, L. K.; Cheung, K. K.; Che, C. M. *J. Chem. Soc., Dalton Trans.: Inorg. Chem.* **1993**, 2933−2938.
(53) Yutaka, T.; Mori, I.; Kurihara, M.; Mizutani, J.; Tamai, N.; Kawai, T.; Irie, M.; Nishihara, H. *Inorg. Chem.* **2002**, *41*, 7143−7150.
(54) Yam, V. W.-W.; Wong, K. M.-C.; Zhu, N. *J. Am. Chem. Soc.* **2002**, *124*, 6506−6507.
(55) Yam, V. W.-W.; Tang, R. P.-L.; Wong, K. M.-C.; Cheung, K.-K. *Organometallics* **2001**, *20*, 4476−4482.
(56) Yam, V. W.-W.; Tang, R. P.-L.; Wong, K. M.-C.; Lu, X.-X.; Cheung, K.-K.; Zhu, N. *Chemistry* **2002**, *8*, 4066−4076.
(57) Yang, Q.-Z.; Wu, L.-Z.; Wu, Z.-X.; Zhang, L.-P.; Tung, C.-H. *Inorg. Chem.* **2002**, *41*, 5653−5655.

by passage through columns of activated alumina and molecular sieves under N_2 as first described by Grubbs.[61]

Characterization. ^{1}H NMR spectra were recorded on a Bruker Avance-400 spectrometer (400.1 MHz), and infrared spectra were obtained from Nujol mulls using a Mattson Galaxy 6020 FTIR spectrometer. Mass determinations were accomplished by electrospray ionization mass spectrometry (ESIMS) using a Hewlett-Packard Series 1100 mass spectrometer (Model A) equipped with a quadropole mass filter. Absorption spectra were recorded using a Hitachi U2000 scanning spectrophotometer (200−1100 nm), and elemental analyses were determined by Desert Analytics, Tucson Arizona.

Luminescence. Luminescence and excitation spectra were obtained using a Spex Fluoromax-P fluorimeter corrected for the spectral sensitivity of the photomultiplier tube and the spectral output of the lamp with monochromators positioned for a 2 nm band-pass. Lifetime measurements were made using a nanosecond laser system previously described.[62] Solution samples were degassed by at least 4 freeze−pump−thaw cycles, and frozen glass samples (1:4 (v/v) MeOH:EtOH) were prepared in NMR tubes placed in a quartz-tipped immersion dewar filled with liquid nitrogen. Thin films were prepared by the spin coating of an CH_3CN solution containing PMMA and $[Pt(NttpyCl)](PF_6)_2$ where the ratio of polymer to complex was approximately 100:1 (w/w). Solid state emission samples were prepared as a 10% mixture (w/w) of the red form of $[Pt(Nttpy)Cl](PF_6)_2$ in a matrix of finely ground KBr contained in resealable J-Young tubes and purged with argon. Solvent vapors for vapochromism studies were generated by vigorously bubbling argon through a sealed 100 mL Erlenmeyer flask containing the anhydrous solvent, and the vapors were transferred to the sample tube via cannulae. Total exposure time of the sample to the vapors was 30 min, and the removal of the vapors was accomplished by gently heating the sample under vacuum.

4′-(*p*-Nicotinamide-*N*-methylphenyl)-2,2′:6′,2″-terpyridine hexafluorophosphate (Nttpy)PF_6. A 250 mL Schlenk tube was charged with Br-ttpy (0.70 g; 1.7 mmol), nicotinamide (0.280 g, 2.29 mmol) and dry acetonitrile. The resulting heterogeneous solution was stirred at reflux for 48 h, filtered through a medium porosity glass frit and the precipitate was washed with diethyl ether. The solid was then collected, dissolved in 20 mL deionized water and a saturated aqueous solution of NH_4PF_6 was added. The resulting heterogeneous solution was stirred for 30 min at room temperature, filtered through a medium porosity glass frit, and the collected solids were washed with water, cold ethanol, and diethyl ether. Yield: 68%. ^{1}H NMR (DMSO-d_6): δ 9.70 (1H, s), 9.36 (1H, d, J = 4 Hz), 9.00 (1H, d, J = 8 Hz), 8.75 (2H, dd, J = 1 Hz, J = 1 Hz), 8.70 (2H, s), 8.67 (2H, d, J = 8 Hz), 8.62 (1H, s), 8.34 (1H, dd, J = 8 Hz, J = 8 Hz), 8.21 (1H, s), 8.05−8.01 (4H, m), 7.80 (2H, d, J = 8 Hz), 7.54 (2H, td, J = 1 Hz, J = 1 Hz, J = 4 Hz), 6.03 (2H, s). ESI MS (+, CH_3CN): *m*/*z* (relative intensity, ion): 444.1, (100, M^+), 401.1, (35, M^+-$CONH_2$).

$[Pt(Nttpy)Cl](PF_6)_2$ (1). A 100 mL 1-neck round-bottom flask was charged with $(Nttpy)PF_6$ (0.8 g, 1.35 mmol), $Pt(DMSO)_2Cl_2$ (0.630 g, 1.49 mmol), and 50 mL of methanol. The resulting solution was heated at 65 °C for 24 h. The solution was then reduced to 25 mL, the resulting solids were collected on a medium porosity glass frit, and washed with cold ethanol and diethyl ether. The material was then dissolved in 50 mL water to which a saturated solution of NH_4PF_6 was added. The resulting heterogeneous solution was allowed to stir for 2 h, and the solids were collected on a medium porosity glass frit and washed with water, ethanol, and diethyl ether. Yield: 74%. ^{1}H NMR (CD_3CN): δ 9.24 (1H, s), 9.08 (2H, d, J = 4 Hz), 8.90 (1H, d, J = 8 Hz), 8.84 (1H, d, J = 8 Hz), 8.50 (2H, s), 8.41 (4H, dd, J = 1 Hz, J = 1 Hz), 8.18 (1H, m), 8.10 (2H, d, J = 8 Hz), 7.89 (2H, m), 7.72 (2H, d, J = 12 Hz), 7.20 (1H, br s), 6.63 (1H, br s), 5.89 (2H, s). FTIR (Nujol): υ(cm^{-1}): 3458 (υ_{CONH_2}), 1703 ($\upsilon_{C=O}$). ESI MS(+, CH_3CN): *m*/*z* (relative intensity, ion): 337.1 (100, M^{2+}). ESI MS (−, CH_3CN): *m*/*z* (relative intensity, ion): 145.1 (100, PF_6^-). Anal. Calcd for $C_{28}H_{22}N_5ClF_{12}OP_2Pt$ (FW = 964.40): C, 34.85; H, 2.29; N, 7.25. Found: C, 35.08; H, 2.38; N, 7.29.

X-ray Structural Determinations of the Orange (1-O) and Red (1-R) Forms of $[Pt(Nttpy)Cl](PF_6)_2$. An orange crystalline sample was grown by the vapor diffusion of diethyl ether into a concentrated solution of **1** dissolved in 1:1 (v/v) acetonitrile:methanol at ambient temperature. A single orange crystal of **1-O** was rapidly mounted under Paratone-8277 oil onto a glass fiber, and immediately placed in a cold nitrogen stream at −80 °C on the X-ray diffractometer. It should be noted that crystals of **1-O** undergo solvent loss at ambient temperature, and the color changes from orange to red (**1-R**). Once data collection was completed, the orange crystal was left on the diffractometer overnight at ambient temperature by which time the color had changed to the red color of **1-R**, and diffraction studies were carried out again. After data collection on this red crystal was complete, the goniometer with the red crystal still attached was exposed to methanol vapors to return the crystal to the orange form **1-O**, and the data collection and refinement processes were repeated. The X-ray intensity data were collected on a standard Bruker-AXS SMART CCD area detector system equipped with a normal focus molybdenum-target X-ray tube operated at 2.0 kW (50 kV, 40 mA). For each structure determination, a total of 1321 frames of data (1.3 hemispheres) were collected using a narrow frame method with scan widths of 0.3° in ω and exposure times of 30 s/frame using a detector-to-crystal distance of 5.09 cm (maximum 2θ angle of 56.6°). The total data collection time was approximately 12 h for each determination. Frames were integrated to a maximum 2θ angle of 56.6° with the Bruker-AXS SAINT program. Laue symmetry revealed triclinic crystal systems for both **1-O** and **1-R**. The final unit cell parameters (at −80 °C) were determined from the least-squares refinement of three-dimensional centroids of >4500 reflections for each crystal. Data were corrected for absorption with the SADABS program.

The space groups were assigned as $\bar{P}1$ (#2) for **1-O** and **1-R**, and both structures were solved by direct methods and refined employing full-matrix least-squares on F^2 (BRUKER-axs, SHELXTL-NT, version 5.10). For both **1-O** and **1-R**, there is one full molecule in the asymmetric unit (Z = 2) and the PF_6^- anions display disorder with the F atoms distributed over two sets of positions around the P atom. All non-H atoms of the cations for both complexes were refined anisotropically and hydrogen atoms were included in idealized positions (the hydrogen atoms of CH_3OH were not included). The structures refined to goodness of fit (GOF) values and final residuals are found in Table 1.

A second red crystal was rapidly mounted under Paratone-8277 oil onto a glass fiber and immediately placed in a cold nitrogen stream at −80 °C on the X-ray diffractometer. Data were collected on this crystal at both 190 and 298 K with each data set being refined as described above, and the results of these studies are given in Supporting Information in CIF format. The CIF file contains three separate structure determinations — one for **1-O** at 193 K, one for **1-R** at 193 K and one for **1-R** at 298 K. Other structure determinations for **1-O** and **1-R** upon the removal or addition of methanol vapor have been conducted but show no differences from those described above and given in CIF format in the Supporting Information.

Results and Discussion

Synthesis and Characterization. The synthesis of the ligand is based upon previously reported methods, and was easily accomplished by the reaction of Br-ttpy and nicotinamide in refluxing acetonitrile followed by counterion metathesis with ammonium hexafluorophosphate as illustrated in Scheme 1.[63] The construction of the ligand involves commercially available

(58) Collin, J.-P.; Guillerez, S.; Sauvage, J.-P.; Barigelletti, F.; De Cola, L.; Flamigni, L.; Balzani, V. *Inorg. Chem.* **1991**, *30*, 4230−4238.
(59) Romeo, R.; Scolaro, L. M. *Inorg. Synth.* **1998**, *32*, 153−158.
(60) Kukushkin, V. Y.; Pombeiro, A. J. L. *Inorg. Synth.* **2002**, *33*, 189−195.
(61) Pangborn, A. B.; Giardello, M. A.; Grubbs, R. H.; Rosen, R. K.; Timmers, F. J. *Organometallics* **1996**, *15*, 1518−1520.
(62) McGarrah, J. E.; Eisenberg, R. *Inorg. Chem.* **2003**, *42*, 4355−4365.

Table 1. Crystallographic, Data Collection and Structure Refinement Parameters for Both Forms of $[Pt(Nttpy)Cl](PF_6)_2$ (**1**)

form	orange (1-O)	red (1-R)
formula	$[Pt(Nttpy)Cl](PF_6)_2 \cdot CH_3OH$	$[Pt(Nttpy)Cl](PF_6)_2$
empirical formula	$C_{29}H_{26}ClF_{12}N_5O_2P_2Pt$	$C_{28}H_{22}ClF_{12}N_5OP_2Pt$
fw	997.03	964.99
T, K	193(2)	193(2)
λ, Å	0.71073	0.71073
crystal system	triclinic	triclinic
space group	$\bar{P}1$(#2)	$\bar{P}1$(#2)
Z	2	2
a, Å[a]	6.7965(7)	6.6479(13)
b, Å[a]	13.8266(14)	13.622(3)
c, Å[a]	18.1411(18)	18.250 (4)
α, β, γ deg[a]	94.816(2), 94.531(2), 96.362(2)	92.781(3), 92.280(3), 97.751(3)
V, Å^3	1681.6(3)	1633.8(6)
ρ_{calcd}, Mg/m^3	1.961	1.962
μ, mm^{-1}	4.451	4.576
abs correction	SADABS[b]	SADABS[b]
transm range	0.49−1.00	0.484−1.00
F(000)	960	932
2θ range, deg	1.78 to 28.26	1.83 to 28.30
limiting indicies	$-8 \le h \ge 9$ $-18 \le k \ge 18$ $-23 \le l \ge 24$	$-8 \le h \ge 8$ $-18 \le k \ge 18$ $-23 \le l \ge 24$
no. of refln's collected	14813	17029
no. of data/restraints/parameters	5941/0/543	6313/0/525
goodness of fit[c]	1.051	1.105
$R1$, $wR2$ ($l > 2\sigma$)[d]	0.0601, 0.1231	0.0472, 0.0914
$R1$, $wR2$ (all data)[d]	0.0862, 0.1313	0.0619, 0.0949

[a] It has been noted that the integration program SAINT produces cell constant errors that are unreasonably small, since systematic error is not included. More reasonable errors might be estimated at 10× the reported value. [b] The SADABS program is based on the method of Blessing; see Blessing, R. H. *Acta Crystallogr., Sect A* 1995, **51**, 33. [c] GOF = $[\sum[w(F_o^2 - F_c^2)^2]/(n - p)]^{1/2}$, where n and p denote the number of data and parameters. [d] $R_1 = (\sum||F_o| - |F_c||)/\sum|F_o|$; $wR_2 = [\sum[w(F_o^2 - F_c^2)^2]/\sum[w(F_o^2)^2]]^{1/2}$ where $w = 1/[\sigma^2(F_o^2) + (a \cdot P)^2 + b \cdot P]$ and $P = [(\max;0,F_o^2) + 2 \cdot F_c^2]/3$.

Scheme 1

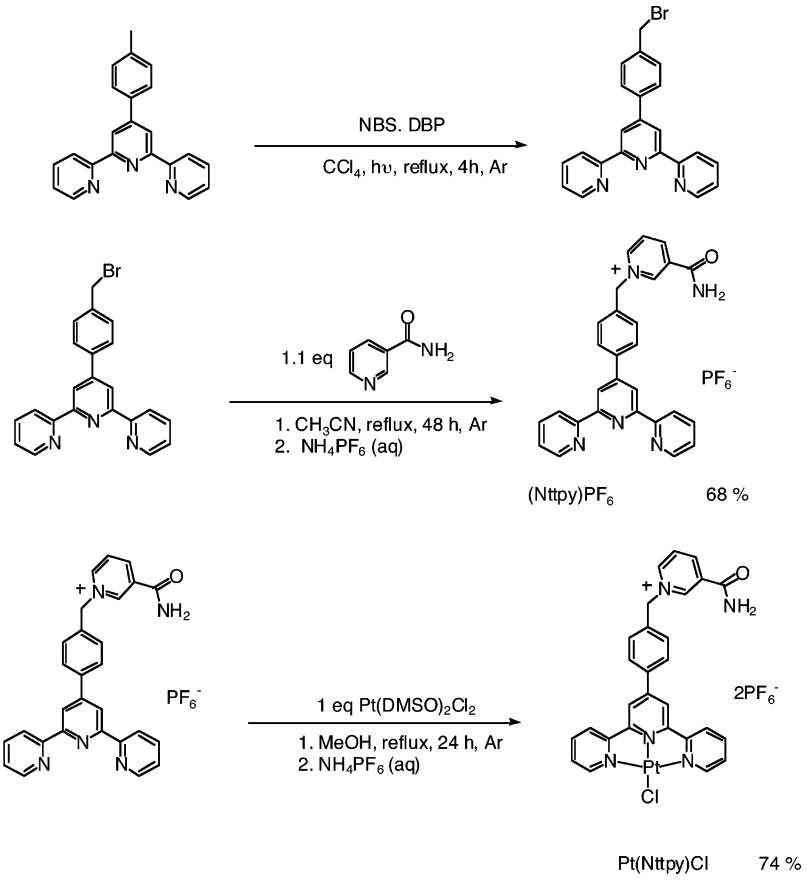

starting materials and requires no chromatography. The synthesis of complex **1** was effected by modification of a previously reported method.[59,60] Because of the solubility properties of the starting materials, a longer reaction time was required and as a

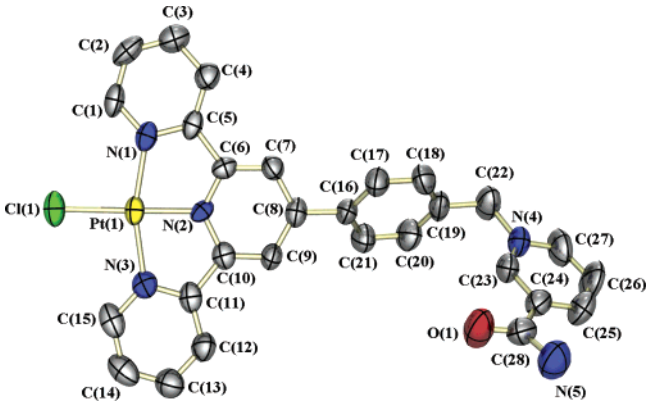

Figure 1. Crystal structure of **1-O**. Anions have been omitted for clarity.

Table 2. Selected Bond Lengths (Å) and Angles (deg) for **1-O** and **1-R**

form	1-O	1-R
Pt(1)−N(1)	2.003(7)	2.016(5)
Pt(1)−N(2)	1.933(6)	1.921(5)
Pt(1)−N(3)	2.033(6)	2.021(6)
Pt(1)−Cl(1)	2.306(2)	2.308(16)
N(1)−C(1)	1.350(9)	1.343(7)
C(1)−C(2)	1.372(11)	1.382(9)
C(8)−C(16)	1.491(11)	1.474(8)
C(17)−C(18)	1.378(12)	1.380(9)
C(19)−C(22)	1.486(12)	1.505(9)
C(22)−N(4)	1.522(11)	1.510(8)
N(4)−C(23)	1.363(11)	1.336(8)
C(23)−C(24)	1.380(11)	1.367(9)
C(24)−C(28)	1.513(12)	1.515(10)
C(28)−O(1)	1.220(11)	1.224(8)
C(28)−N(5)	1.325(11)	1.317(9)
N(1)−Pt(1)−N(2)	80.9(3)	81.27(19)
N(2)−Pt(1)−N(3)	81.1(3)	80.86(19)
N(1)−Pt(1)−N(3)	161.9(3)	162.13(19)
N(2)−Pt(1)−Cl(1)	179.43(18)	179.14(14)
C(19)−C(22)−N(4)	113.8(7)	113.5(5)
C(24)−C(28)−N(5)	117.4(8)	117.6(7)
C(24)−C(28)−O(1)	119.1(8)	118.8(6)
O(1)−C(28)−N(5)	123.4(9)	123.5(7)

result, $Pt(DMSO)_2Cl_2$ and the ligand $[Nttpy]PF_6$ were heated at 65 °C for 24 h in MeOH. The reaction was observed to run heterogeneously and the product was isolated by simple filtration followed by a second counterion metathesis with ammonium hexafluorophosphate. Complex **1** was observed to be soluble in a limited number of organic solvents including MeOH, CH_3CN, DMF, and DMSO, and was characterized by ^1H NMR, FTIR, ESIMS, and elemental analysis. The spectroscopic data are consistent with a dicationic Pt(II) complex having a square planar geometry with three of the four coordination sites occupied by a nicotinamide-modified terpyridyl ligand and the fourth site occupied by chloride. Single-crystal X-ray diffraction studies support this assignment.

Crystal Structures of 1-O and 1-R. The crystal structures of both the orange and red forms of **1** have been determined by X-ray diffraction and the molecular structure of the cationic Pt(II) complex for **1-O** is shown in Figure 1 (the cationic complex in **1-R** is essentially identical). Table 2 lists important bond lengths and angles for both the orange (**1-O**) and red (**1-R**) crystalline forms. The distorted square planar geometry is

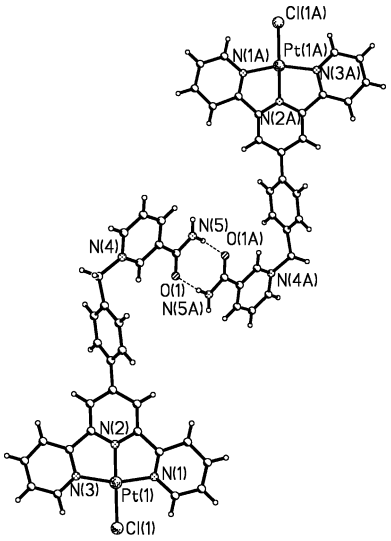

Figure 2. Dimeric form of **1-R** depicting the hydrogen bonding that occurs in the solid state.

evidenced by a N(1)−Pt−N(3) 'trans' angle of 162.1(3)° for **1-O** and Pt−N distances that range from 1.919 (8) to 2.037 (9) Å with the central nitrogen having the shortest distance. The Pt−Cl bond distance is 2.303(3) Å. All bond lengths and angles agree well with other structural reports of platinum terpyridine complexes found in the literature.[32,41−43,45,50−52,54,55,64,65]

Analysis of the crystal packing of **1-O** reveals that the molecules are stacked in a head-to-tail orientation with the cations existing as hydrogen-bonded dimers in the solid state. The hydrogen bonding which is shown in Figure 2 occurs between the amide groups of two complexes in different stacks with the N−H···O distance being 2.913(5) Å. Figures 3 and 4 depict the crystal packing of **1-O** where alternating distances are observed between adjacent Nttpy ligands and Pt atoms. The distances of 3.763 and 3.692 Å between the terpyridyl ligands indicate very small-to-negligible $\pi-\pi$ interactions while the Pt···Pt distances alternate between 3.622 and 3.964 Å with a zigzag geometry shown by a Pt···Pt···Pt angle of 126.7°. The distances and nonlinearity of the arrangement between neighboring Pt atoms do not allow for effective overlap of nearest neighbor Pt d_{z^2} and p_z orbitals that are the basis of metallophilic interactions. Solvent molecules of methanol were found to reside within voids between the stacked cations but no large cavities were observed in the crystal structure. The methanol molecules exhibit weak hydrogen bonding with the amide NH_2 of a neighboring nicotinamide, the O···H−N distance also being 3.122 (2) Å.

The overall structure of **1-R**, determined from the *same* crystal, is very similar to that of **1-O**. However, a close inspection of the packing diagram in Figure 3 reveals a distinct difference between the solid-state packing in the red and orange forms. As with **1-O**, hydrogen bonding occurs between the amide groups of two Nttpy ligands to form dimers between complexes located in two different stacks with an N−H···O distance of 2.890 Å. Large cavities are also absent within the crystal lattice of **1-R** but unlike **1-O**, methanol is not observed in the void space between the stacked cations. The main

(63) Yamaguchi, N.; Nagvekar, D. S.; Gibson, H. W. *Angew. Chem., Int. Ed. Engl.* **1998**, *37*, 2361−2364.
(64) Yam, V. W.-W.; Wong, K. M.-C.; Zhu, N. *J. Am. Chem. Soc.* **2002**, *124*, 6506−6507.
(65) Jude, H.; Bauer, J. A. K.; Connick, W. B. *J. Am. Chem. Soc.* **2003**, *125*, 3446−3447.

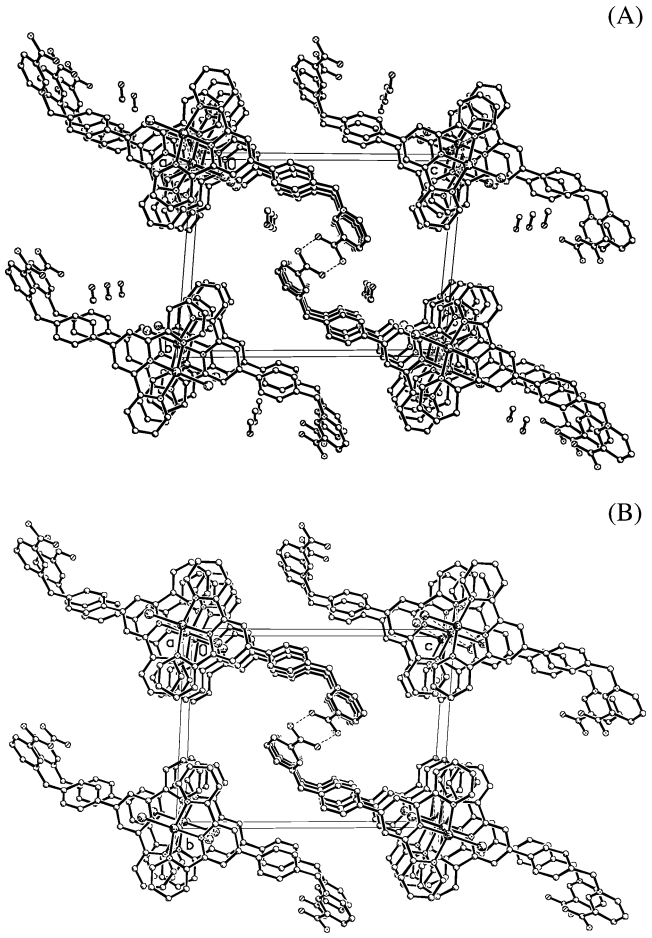

Figure 3. Solid-state packing diagrams of **1-O** (A) and **1-R** (B) showing the presence of methanol within the lattice of **1-O**. In both cases, anions have been omitted for clarity.

difference in the solid-state packing between **1-O** and **1-R** is found in the interplanar Nttpy···Nttpy and Pt···Pt separations for the two forms. As shown in Figure 4, the intermolecular separation between the Nttpy ligands alternates between 3.453 and 3.660 Å. The former is well below 3.8 Å which is normally considered the upper limit for $\pi-\pi$ interactions between organic molecules.[66,67] Analysis of the packing also reveals that the Pt···Pt distances between neighboring complexes are significantly shorter with distances alternating between 3.301 and 3.360 Å. Although larger than those observed for bimetallic $Pt_2(trpy)_2(\mu\text{-L})$ complexes, they are well within the expected range of metal−metal distances observed for other $Pt(ttpy)Cl^+$ salts.[41−43,45,52,68] The Pt···Pt···Pt arrangement is also more linear in **1-R** than in **1-O** with a Pt···Pt···Pt angle of 171.9°, thereby helping to promote overlap between d_{z^2} and p_z orbitals on neighboring complexes leading to the observed color difference between the two forms (vide infra).

Single-crystal transformations that involve loss and/or gain of solvent molecules while maintaining the integrity of the crystal lattice are rare.[69−71] In the present case, this transformation and the ability to characterize each form structurally and spectroscopically provided a valuable opportunity to study the relationship between molecular structure and excited-state energy.

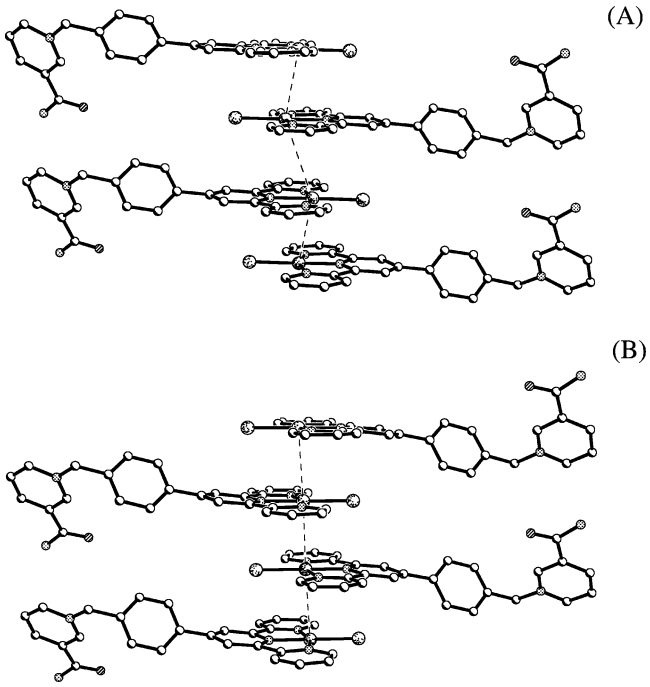

Figure 4. Comparison between the molecular stacking diagram depicting the nonlinear (126.7°) angle between Pt atoms in **1-O** (A) and the pseudolinear (171.9°) arrangement in **1-R** (B). Methanol molecules are removed for clarity in A.

Electronic Absorption and Emission Spectroscopy. The absorption spectrum of $[Pt(Nttpy)Cl](PF_6)_2$ was measured at room temperature in acetonitrile and the spectrum is shown in Figure 5. The spectrum displays many similarities to the absorption spectra for other $[Pt(ttpy)Cl]^+$ complexes that have been previously reported.[48,72] The structured bands between 250 and 350 nm are assigned to $^1(\pi-\pi^*)$ transitions associated with the coordinated Nttpy ligand. The transitions at lower energy (350−450 nm) are assigned to MLCT transitions which result from the promotion of an electron from a Pt(d) HOMO to the LUMO which is a π^* orbital on the terpyridyl ligand.

The complex is not emissive in fluid solution at room temperature but does display intense luminescence in a rigid matrix, and this is depicted in Figure 5. When the complex is prepared in a 4:1 ethanol:methanol glass, an intense, highly structured emission is observed between 500 and 650 nm that contains three components with maxima at 508, 545, and 585 nm. The vibronic spacing between the 0−0 and 0−1 transitions is 1200 cm^{-1}, while the Huang−Rhys factor defined as the I_{01}/I_{00} is approximately 0.9 suggesting that the emission arises from a minimally distorted excited state of $\pi-\pi^*$ or $Pt(d)-\pi^*(Nttpy)$ charge-transfer character.[41−43,45] This spectral profile is analogous to the emission spectra of dinuclear Pt terpyridine complexes and $Pt(4'R\text{-trpy})Cl^+$ salts where R contains an electron donating substituent like NMe_2.[46,49] The lifetime

(66) Hunter, C. A.; Meah, M. N.; Sanders, J. K. M. *J. Am. Chem. Soc.* **1990**, *112*, 5773−5780.
(67) Hunter, C. A.; Sanders, J. K. M. *J. Am. Chem. Soc.* **1990**, *112*, 5525−5534.
(68) Yip, H. K.; Che, C. M.; Zhou, Z. Y.; Mak, T. C. W. *J. Chem. Soc. Chem. Commun.* **1992**, 1369.
(69) Rather, B.; Zaworotko, M. J. *J. Chem. Soc., Chem. Commun.* **2003**, 830−831.
(70) Lu Jack, Y.; Babb Amy, M. *J. Chem. Soc., Chem. Commun.* **2002**, 1340−1341.
(71) Biradha, K.; Fujita, M. *Angew. Chem., Int. Ed.* **2002**, *41*, 3392−3395.
(72) Michalec, J. F.; Bejune, S. A.; Cuttell, D. G.; Summerton, G. C.; Gertenbach, J. A.; Field, J. S.; Haines, R. J.; McMillin, D. R. *Inorg. Chem.* **2001**, *40*, 2193−2200.

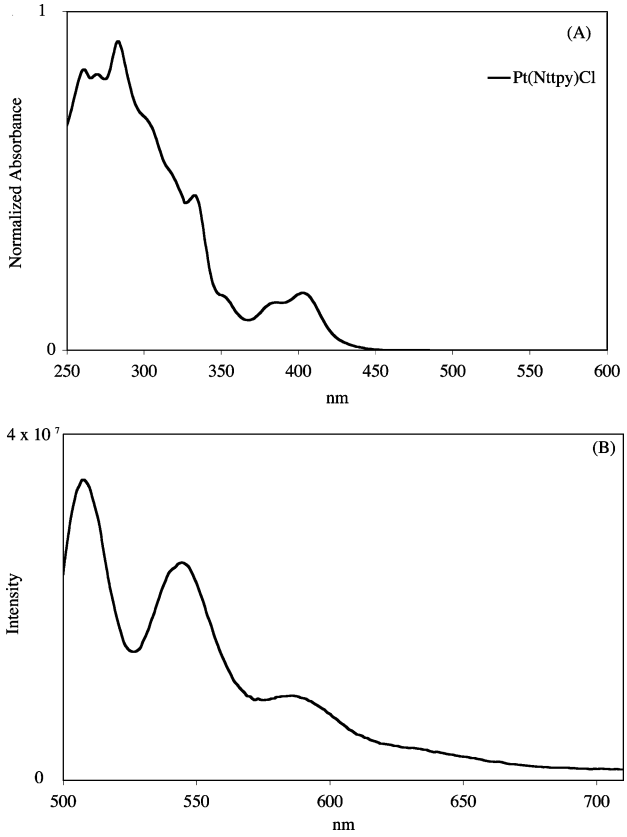

Figure 5. (A) Room-temperature absorption spectrum of **1** in degassed acetonitrile. (B) 77 K emission of **1** in a 4:1 EtOH:MeOH glass.

measured at 77 K in a 4:1 EtOH:MeOH frozen glass was fit to a single-exponential decay and is observed to be 20 μs, suggestive of triplet character for the emissive state.

Both crystalline and powdered samples of the red and orange forms of **1** were found to be interconvertible by exposure to and removal of methanol vapors. The solid-state emission spectra of **1-R** and **1-O** were measured at ambient and low temperatures and are presented in Figure 6. At room temperature **1-R** is observed to be brightly emissive and displays a broad structureless emission with an emission maximum of 660 nm and an excited-state lifetime of 0.09 μs. The excited state that gives rise to this emission is assigned as a metal-to-ligand charge-transfer involving Nttpy π* as the LUMO. The metal-based HOMO in **1-R** is affected by Pt···Pt interactions and corresponds to a dσ* function formed by overlapping d_{z^2} orbitals that are formally antibonding with regard to the Pt···Pt interaction. In light of this metal−metal interaction, the emissive state of **1-R** is thus designated as ^{3}MMLCT.

From Table 3, it can be clearly seen that upon cooling to 77 K the emission maximum of **1-R** red-shifts to 701 nm while the intensity and excited state lifetime increase approximately 1.5 and 10-fold, respectively. The increases in emission intensity and lifetime are due to reduction of nonradiative decay rates upon cooling. In addition, the spectral profile of **1-R** narrows considerably based on a full width-at-half-maximum (fwhm) analysis, going from 1856 cm^{-1} at 298 K to 831 cm^{-1} at 77 K. The changes in the spectral profile as well as the emission energy upon cooling are due to lattice contraction within the bulk solid, leading to a decreased Pt···Pt distance and a lowering of the dσ*-π*(Nttpy) energy gap. X-ray diffraction analysis

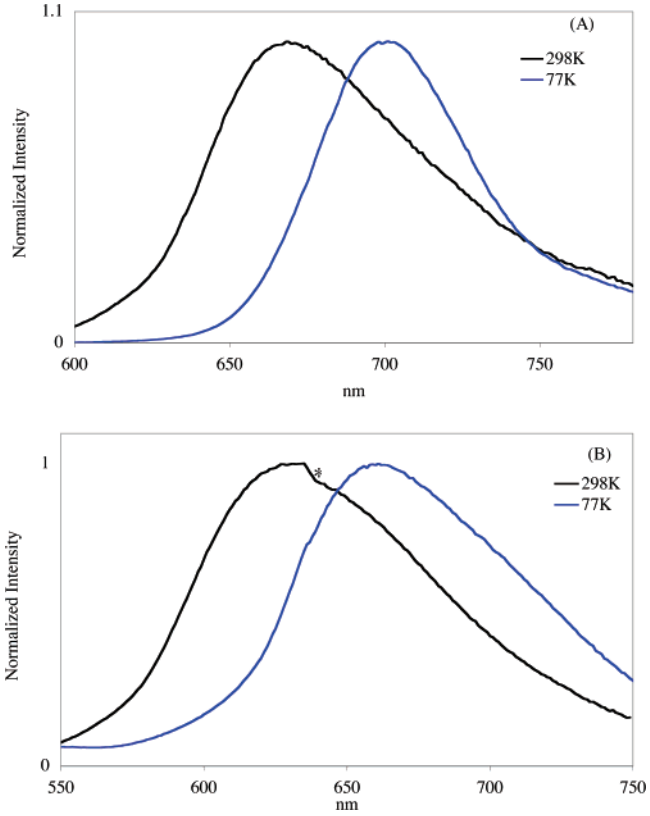

Figure 6. Solid-state emission of **1-R** (A) and **1-O** (B) at 298 and 77 K. * denotes instrumental artifact.

Table 3. Solid State Photophysical Data for **1-O** and **1-R**

form[a]	λ_{em}^{max} (nm) 298 K/77 K	τ (μs) 298 K/77 K	fwhm (cm^{-1}) 298 K [77 K]
orange	630/660	0.19/1.94	2461 [2136]
red	660/700	0.09/0.94	1856 [831]

[a] Data collected as a 10% (w/w) mixture in anhydrous KBr.

conducted on single crystals of **1-R** at 193 and 298 K (see Supporting Information) indicate that the Pt···Pt distance is approximately 0.027 Å shorter at the lower temperature, consistent with the observed red-shift in emission on cooling (see Supporting Information). Although the observed decrease in Pt···Pt separation is small, it is significant enough to cause the emission maximum to shift to lower energy when the sample is cooled. The photophysical and crystallographic results at 298 and 193 K clearly illustrate the importance of Pt···Pt interactions in the ^{3}MMLCT emissive state.

The emission spectrum of **1-O** is also broad and structureless with an emission maximum of 630 nm, and an excited-state lifetime of 0.19 μs. Upon cooling to 77 K an increase in intensity is observed concomitant with a 10-fold increase in excited-state lifetime, and the emission maximum is also seen to red-shift to 660 nm. These spectral changes are similar to those observed with **1-R**. However, the emission profile is not seen to significantly narrow (Table 3) based on fwhm analysis. On the basis of the crystal structure analysis of **1-O**, Pt···Pt interactions are much weaker than for **1-R** and the excited state is thus more properly assigned to be ^{3}MLCT without perturbation from metallophilic bonding. Typical emission energies for ^{3}MLCT transitions found in other Pt polypyridine complexes are significantly blue shifted to that observed in the present study

for **1-O**. The lower energy ^{3}MLCT emission seen here is thought to result from an inductive effect exerted by the nicotinamide substituent of the Nttpy ligand. Although not in resonance with the rest of the Nttpy ring system, this positively charged substituent lowers the energy of the Nttpy based LUMO resulting in emission that is distinctly shifted to lower energy, although not as extensively as is found for **1-R** in which the HOMO is raised in energy through Pt···Pt bonding. Interestingly, low energy emissions have recently been reported in fluid solution for a series of Pt(trpy) acetylide complexes,[54] but these may be red-shifted because of the influence of acetylide relative to chloride on the Pt d orbital energies.

To further probe the existence of metal−metal interactions and their influence on the emission properties of complex **1**, thin films of **1** were spin coated onto ITO glass and the emission properties of the films were examined. The emission profile of the film is highly structured with a $\lambda_{max}^{em} = 526$ nm (see Supporting Information). The polymer matrix prevents any metallophilic interactions that would result in a lower energy emission, thus supporting the notion that the red color of **1-R** in both absorption and emission occurs as a result of Pt···Pt interactions in the solid state.

Vapochromic Behavior of Pt(Nttpy)Cl$^+$. When [Pt(Nttpy)Cl](PF$_6$)$_2$ is devoid of solvent, the emission maximum of red crystalline **1-R** occurs at 660 nm at room temperature. Upon exposure of **1-R** to methanol vapors under ambient temperature, a rapid vapochromic response is observed in which the solid changes to the orange color of **1-O** with a shift of λ_{em}^{max} to 630 nm (Figure 7a). The visual emission change is shown in Figure 7b. A 1.5-fold increase in emission intensity is also observed, coincident with a doubling of the excited-state lifetime to 0.19 μs. This vapochromic response is fully reproducible with conversion from **1-O** back to **1-R** accomplished by heating the sample under vacuum or leaving it exposed to the ambient atmosphere. In Figure 7c, this cycle is repeated five times, and it has been repeated many more times without chemical degradation of the sample. With a powder sample of **1-R**, X-ray diffraction shows that the lattice changes slightly upon exposure to MeOH vapor as the color changes to orange and then returns to its original form upon purging the sample with air at ambient temperature (see Figures S-3 and S-4 in Supporting Information). The powder pattern of **1-R** matches the powder pattern calculated for **1-R** based on the single-crystal structural results (see Figure S-5 in Supporting Information).

The observed vapochromic behavior correlates with the structural changes that occur within the crystal lattice and can be explained as follows. The crystal packing observed in the red form of complex **1** demonstrates that the Pt ions are stacked in a pseudolinear fashion with a Pt···Pt···Pt angle of 171.9° and an average Pt···Pt separation of 3.33 Å allowing for effective overlap of the Pt d_z^2 orbitals between adjacent complexes. While the orbital character of the LUMO is unperturbed (or only slightly perturbed) in going from **1-O** to **1-R**, the nature of the HOMO changes from a Pt d orbital localized on discrete complexes to a dσ* function which results from the metallophilic interaction. The immediate effect of this higher energy HOMO results in the lowering of the HOMO−LUMO energy gap and an increase in λ_{em}^{max} of the emission.

In the opposite direction, when a crystal of **1-R** is exposed to MeOH vapors, the sorption of MeOH causes an expansion

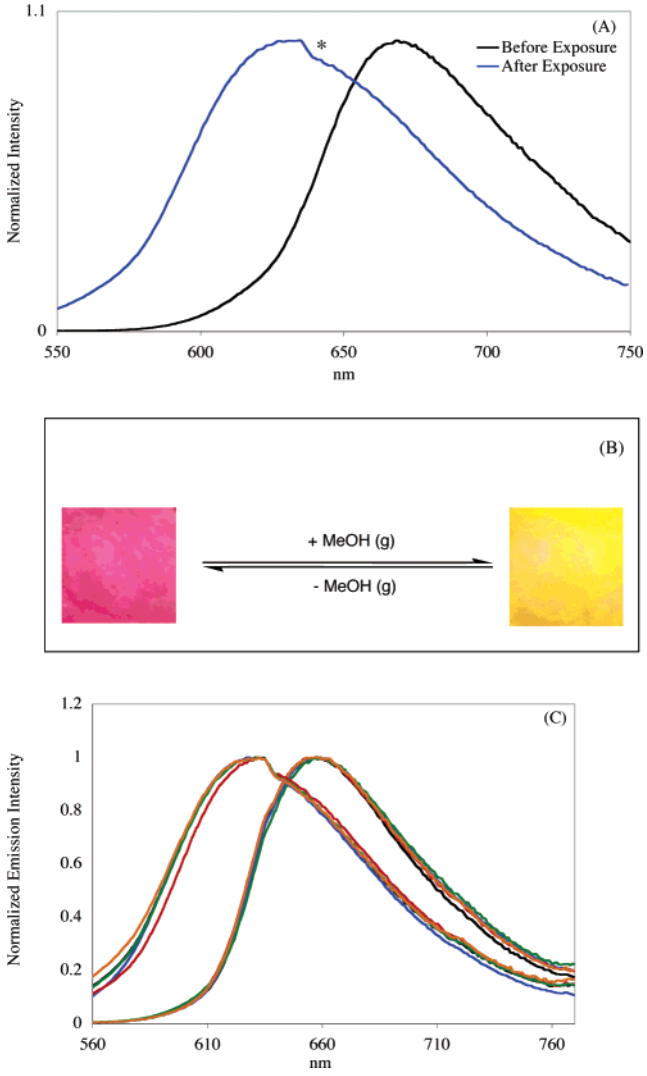

Figure 7. (A) Normalized room-temperature solid-state emission spectrum of **1** before and after exposure to MeOH vapors. * denotes instrumental artifact; (B) Luminescence of **1** as observed by eye in the presence and absence of MeOH vapors. The complex is immobilized on filter paper and irradiated under long wave UV-light at room temperature; (C) Emission results obtained from cycling through exposure to and removal of MeOH vapor in air multiple times.

of the crystal lattice, effectively disrupting the overlap of the Pt d_z^2 orbitals. This is evidenced by the change in Pt···Pt···Pt angle and average Pt···Pt separation to 126.7 ° and 3.79 Å, respectively, from values of 171.9 ° and 3.33 Å found in the red form (Figure 4). Disruption of the metallophilic interactions thus induces a change in the nature of the HOMO which in **1-O** is predominately localized on a single Pt center, leading to an increase in the HOMO−LUMO gap as observed experimentally.

To ensure that this response was not a property of surface effects resulting from grinding the crystals with KBr for sample preparation, samples containing only large crystals of **1-R** were exposed to methanol vapors in an analogous manner. Within 10 min, the color of the crystals changed from red to orange, and this process was also reproducible and reversible. The slower vapochromic response of the macro-crystalline sample relative to that of the dispersed powder merely reflects differences in the exposed surface area and the time needed for the vapors to penetrate the larger crystalline samples. As mentioned

above, the powder pattern of **1-R** agrees closely with that calculated for **1-R** based on the single-crystal data while similar correspondence is seen between experimental and calculated powder patterns for **1-O**.

A qualitative examination of the vapochromic response of $Pt(Nttpy)Cl^+$ for other solvents was also explored by exposing microcrystalline samples of **1-R** immobilized on filter paper to various organic solvents. The complex is very selective in this regard, yielding a positive vapochromic response only for pyridine of the solvents tried, in addition to methanol and acetonitrile (Table S1). The vapochromic response is slowest for pyridine consistent with its larger size and lower volatility (C_5H_5N: 20.68 Torr at 298 K).[73]

Complex **1** demonstrates a much more selective response than other complexes that exhibit vapochromic behavior. For comparison, Mann's Pt double salts demonstrate a vapochromic response to alcohols, organic acids, polar aprotic solvents, halocarbons and aromatic solvents.[10−19] Unlike cyclometalated Pt(II) complexes based on 2,6-diphenylpyridine, the changes in the photophysical properties of **1** upon exposure to solvent vapors are readily observed. This system may possess interest as a sensory material[74] since its mode of detection does not rely on the quenching of luminescence but rather on a change in emission energy and consequent sample color. At this point, however, the factors that influence and control a positive vapochromic response in $Pt(Nttpy)Cl^+$ require further study.

The most extraordinary aspect of the present study is that the vapochromism of **1** has been examined on *individual* crystals that have been *structurally* characterized in each form. In essence, the sorption of methanol into the lattice of **1** and its effect on intermolecular interactions as well as resultant absorption and emission bands has been observed directly. Although the specific nonbonded contacts of methanol that are causative in altering the crystal structure of **1** are not entirely clear, the combination of X-ray and spectroscopic results provide unambiguous evidence of the effects of sorption and desorption into the crystals of this vapochromic system while maintaining its crystallinity. In this regard, crystals of **1** exhibit similarities to $Ni_2(bpy)_3(NO_3)_4 \cdot 2$ ROH (bpy = 2,2′-bipyridine; R = Me, Et) that provide a porous metal-organic structure in which methanol sorption has been followed and suggested to proceed by scissoring motions in the lattice without disrupting crystallinity.[75−77] In the present case, the lattice remains intact while the stacked planar complexes undergo slippage and slight separation relative to each other to accommodate the MeOH adsorbate.

Conclusion. The crystal structure of both the red and orange forms of $Pt(Nttpy)Cl^+$ have been determined from X-ray diffraction studies on the same single crystal. Analysis of the packing confirms that the red form possesses significant metal−metal interactions with Pt atoms arranged in a nearly linear chain, but the orange form contains Pt atoms that are further apart with Pt···Pt distances of 3.622 and 3.964 Å and a Pt···Pt···Pt angle of 126.7 °. These spatial and geometric differences explain the distinct color changes between the two forms and the different photophysical properties between them. The red form's photophysical properties arise from a ^{3}MMLCT excited state involving a HOMO influenced by Pt···Pt interaction, whereas the orange form's photophysical properties result from a ^{3}MLCT charge transfer excited state originating from discrete complexes. The complex displays a selective vapochromic response when exposed to MeOH, CH_3CN and pyridine, and this response can be rationalized from the crystal structure analyses. The vapochromic behavior is highly reversible and can be accomplished without major alteration of the crystal lattice of **1**. Current efforts focus on synthesizing other vapochromic complexes, understanding the factors eliciting a vapochromic response and tuning the specificity of that response for possible sensor application.

Acknowledgment. We wish to thank the Department of Energy, Division of Basic Sciences for support of this research, Dr. Cavan Fleming for his assistance in collecting solid-state lifetime data, and Professor William C. Connick of the University of Cincinnati for helpful comments.

Supporting Information Available: Crystal data, atomic coordinates, bond distances, bond angles, anisotropic displacement parameters and the effects of temperature on the crystal lattice of **1** (deposited in CIF format), the emission of **1** in a PMMA film, the emission spectra of **1-R** at 190 and 298 K, and X-ray power diffraction results for **1-R** and **1-O** are available free of charge via the Internet at http://pubs.acs.org. The CIF file contains three separate structure determinations—one for **1-O** at 193 K, one for **1-R** at 193 K and one for **1-R** at 298 K. This material is available free of charge via the Internet at http://pubs.acs.org.

JA047955S

(73) Ohe, S. *Computer-Aided Data Book of Vapor Pressure*; Elsevier: New York, 1976.
(74) Lu, W.; Chan, M. C. W.; Cheung, K. K.; Che, C. M. *Organometallics* **2001**, *20*, 2477−2486.
(75) Fletcher, A. J.; Cussen, E. J.; Prior, T. J.; Rosseinsky, M. J.; Kepert, C. J.; Thomas, K. M. *J. Am. Chem. Soc.* **2001**, *123*, 10001−10011.
(76) Cussen, E. J.; Claridge, J. B.; Rosseinsky, M. J.; Kepert, C. J. *J. Am. Chem. Soc.* **2002**, *124*, 9574−9581.
(77) Fletcher, A. J.; Cussen, E. J.; Bradshaw, D.; Rosseinsky, M. J.; Thomas, K. M. *J. Am. Chem. Soc.* **2004**, *126*, 9750−9759.